



**HAL**  
open science

## Modulation of the cathode potential of a 100 W-class Hall thruster IEPC

Vincent Delbosq, Stéphane Mazouffre, Milan Tichý, Pavel Kudrna

► **To cite this version:**

Vincent Delbosq, Stéphane Mazouffre, Milan Tichý, Pavel Kudrna. Modulation of the cathode potential of a 100 W-class Hall thruster IEPC. 38th International Electric Propulsion Conference, Jun 2024, Toulouse, France. pp.282. hal-04668752

**HAL Id: hal-04668752**

**<https://hal.science/hal-04668752v1>**

Submitted on 7 Aug 2024

**HAL** is a multi-disciplinary open access archive for the deposit and dissemination of scientific research documents, whether they are published or not. The documents may come from teaching and research institutions in France or abroad, or from public or private research centers.

L'archive ouverte pluridisciplinaire **HAL**, est destinée au dépôt et à la diffusion de documents scientifiques de niveau recherche, publiés ou non, émanant des établissements d'enseignement et de recherche français ou étrangers, des laboratoires publics ou privés.

# Modulation of the cathode potential of a 100 W-class Hall thruster

IEPC-2024-282

*Presented at the 38th International Electric Propulsion Conference, Toulouse, France  
June 23-28, 2024*

Vincent Delbosq\* and Stéphane Mazouffre†  
*CNRS, ICARE laboratory, 45071 Orléans, France*

Milan Tichý and Pavel Kudrna  
*Charles University, Prague, Czech Republic*

**Abstract:** Due to unparallel characteristics in term of thrust-to-power ratio, specific impulse, efficiency and lifetime, Hall thrusters (HT) have attracted a great deal of interest for the scientific community and companies involved in the privatization of space. Numerous studies have been and are being conducted to better understand Hall thruster physics and functioning and to increase performance and operational life. The discharge study is a case in point. Indeed, stabilizing and controlling the oscillations of the discharge current has an impact on thruster performance and lifetime. The aim of this study is twofold, namely: to develop an approach for modulating the discharge current and to investigate the effect of the modulation on discharge properties. We conducted experiments on the ISCT-100 thruster, a 100 W-class HT. An electronic circuit was designed to amplify an harmonic voltage signal and generate two outputs in phase opposition. The voltage difference between the cathode emitter and the keeper was chosen to control oscillations in the discharge current. A broad range of frequencies and amplitudes has been examined, which covers the breathing mode, axial transit time oscillations, and high-frequency oscillations in the MHz domain.

## Nomenclature

$HT$	= Hall thruster
$GIE$	= gridded ion engine
$I_d$	= discharge current
$I_e$	= electron current
$I_i$	= ion current
$V_f$	= floating potential
$V_p$	= plasma potential
$V_e$	= input voltage

---

\*Electric Space Propulsion Research Engineer, ICARE, CNRS, vincent.delbosq@cnrs-orleans.fr.

†Research Director, ICARE, CNRS, stephane.mazouffre@cnrs-orleans.fr.

# I. Introduction

## A. Electric Propulsion

ELECTRIC propulsion is a technology that uses an ionized gas to move artificial satellites, such as probes and satellites. During the Cold War space race between the USSR and the USA in the 1960s, two types of propulsion were developed: gridded ion engines (GIE) in the US and Hall thrusters (HT) in the USSR. One of the first functional application of electric propulsion took place in 1971 when Soviet Meteor weather satellites used SPT-60s (Stationary Plasma Thrusters) for orbit correction. In 1998, the Deep Space 1 probe became the first scientific probe to be equipped with an electric thruster as the main propulsion system. The Smart 1 lunar probe, powered by Safran PPS®1350 Hall thruster, followed in 2003. Electric propulsion has not been widely used in the late 90s and early 2000s due to the time required to achieve large velocity increments. Electric propulsion takes between 3 and 6 months to reach geosynchronous orbit, whereas conventional (chemical) propulsion takes around ten days. As a result, until the 2010s, it was sidelined by companies. The democratization of access to space has led to a diversification of supply and demand, resulting in the emergence of new players, such as start-ups, offering propulsion adapted to micro and nano satellites, alongside traditional manufacturers. Private players view it as advantageous due to its weight savings for satellites and its large velocity increment capabilities despite its low thrust (less than  $1N$ ). This democratization reflects the maturity of the technology, thanks to the work of scientists.

There are three main classes of electric propulsion available. They correspond to the three forces used to accelerate ions: electrothermal, electrostatic and electromagnetic. Hall thrusters are generally regarded as electrostatic systems, since thrust is generated by ions accelerated in an electric field.

## B. Hall thruster

Hall thrusters use both an electric and magnetic field to limit electron movement and ionize gas. Hall thrusters are currently the most popular choice due to their effectiveness and efficiency. This is one of the oldest technologies, which requires a thorough understanding of system physics. The Starlink constellation exemplifies the dominance of these thrusters.

The Hall thruster is a gridless ion accelerator that takes the form of a ring with coils or permanent magnets at its center and periphery. To accelerate the ions, they must first be generated. To accomplish this, the selected propellant (such as xenon) is introduced through the anode and then ionized by a confined discharge of high-energy electrons that occurs in the ceramic annular channel, see Fig. 1. The majority of the resulting ions have a single positive charge, but a significant proportion are doubly charged, as noted by S. Tsikata, I. Katz, and S. Kim.<sup>1-3</sup> After the creation of these ions, they are accelerated by a strong electric field ( $E$ ) before being expelled. The speed of the ions, which can reach 20 to 30 km/s depending on the strength of the  $E$  field, is responsible for the thrust force due to conservation of momentum. To maintain electrical neutrality in the ion beam, a neutralizer is present.

The neutralizer provides electrons to neutralize the ion beam and to maintain the plasma discharge inside the channel. The neutralizer is here a hollow cathode fed with a small fraction of propellant gas. Electron production is enhanced thanks to a  $LaB_6$  solid emitter. Electrons traveling towards the anode must pass through a radial magnetic field, which confines them and enables proper gas ionization.

The magnetic field must ensure that the Larmor radius of the electrons is smaller than the dimensions of the dielectric channel. The  $B$  field should not affect the ions. The electrons are trapped in orbit around the field lines by the Lorentz force at the HT exit plane. According to S. Mazouffre,<sup>4</sup> the electron mobility transverse to the  $B$  field lines decreases sharply. To maintain the electron current ( $I_e$ ), an intense axial electric field of several 100V/cm<sup>4</sup> appears at the exit plane of the thruster, as the applied potential difference is concentrated in the region where the electrons are slowed down.

The presence of two fields generates a strong azimuthal electron current, known as the Hall current, in the dielectric channel. This leads to highly efficient propellant ionization (90%).

To sum up, Hall thrusters utilize an  $E \times B$  configuration to ionize neutral gas and generate thrust. Various studies on this type of thruster have highlighted different instabilities, ranging from kHz to MHz. It is important to note that not all oscillations are detrimental to thruster performance. Plasma and discharge instabilities are significant factors in propellant ionization and ion acceleration. The breathing mode is the dominant instability in Hall thrusters within this frequency spectrum. The main oscillations<sup>5</sup> in a Hall

thruster are as follows:

- Low frequency ionization oscillations:<sup>6</sup> Breathing mode (10-20 kHz).
- Azimutal low frequency oscillations (kHz range).
- Axial ion transit time oscillations: 100-500 kHz range.
- High-frequency instabilitiy (e.g.  $E \times B$  electron drift): 1-10 MHz range.

### C. Objectives

In this contribution we present experimental works on perturbation of the plasma discharge of a low-power Hall thruster. The objective is to operate the thruster in a forced-regime and to investigate the impact of the perturbation on both the plasma properties and the thruster characteristics. There are two ways to easily perturb the discharge of Hall thrusters, namely: anode potential modulation<sup>7-9</sup> or cathode potential modulation.<sup>10-13</sup> We decided to pursue the latter, where at the selected frequency the cathode current, hence the discharge current is modulated.

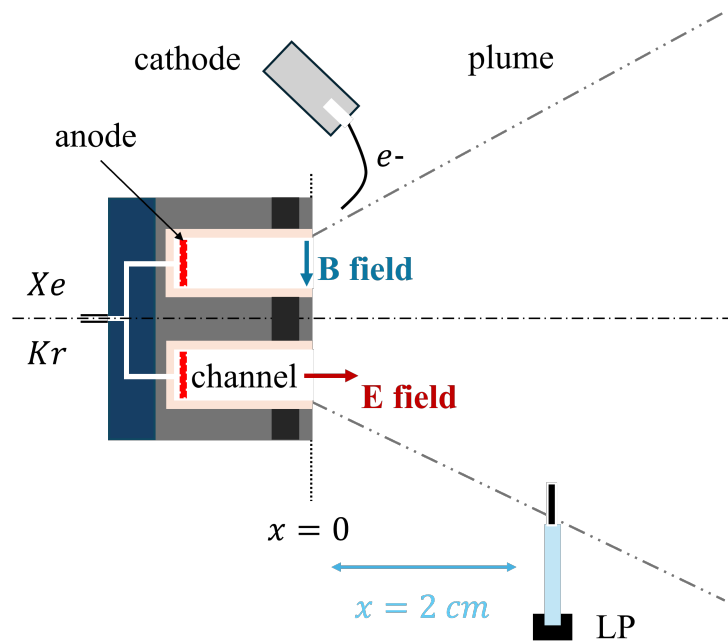


Figure 1. Layout of the experimental setup (not to scale).

## II. Experimental setup

### A. ISCT-100-V3

The ISCT-100-V3 (Icare Small Customizable Thruster) is a 100 W-class thruster capable of operating with xenon [Fig. 2] or krypton and is the successor of the ISCT-100-V2,<sup>14</sup> which offers similar performance to the Busek-BHT-100.<sup>15</sup> It is the latest HT to be developed (2018) in the "ISCT" series, launched in the late 2010s by the EP Team at the ICARE laboratory. This series is the result of extensive research into the miniaturization of thrusters in response to market trends, particularly those related to microsats, nanosats, or cubesats. The ISCT-100-V3 is the laboratory model of the ExoMG<sup>TM</sup>-micro thruster from Exotrail. It delivers solid performance with xenon:<sup>16</sup> 75 mN thrust, equivalent to 0.75 g mass on Earth, 1350 ISP and 39% anode efficiency at 130 W.

During the study, a LaB<sub>6</sub> hollow cathode positioned on the upper-right hand side of the thruster as a neutralizer is used. It supplies the electron current required to balance the plasma discharge and neutralize

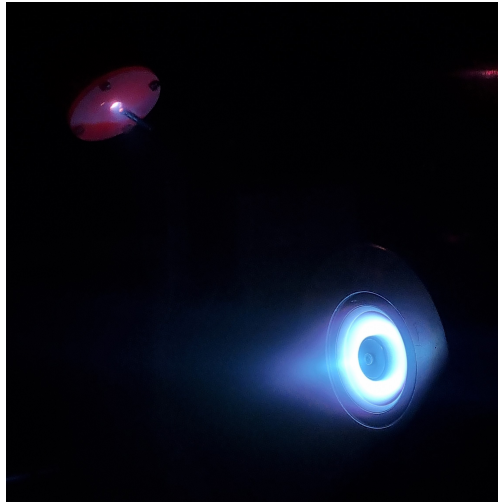


Figure 2. ISCT-100-V3 firing w/ xenon in the NExET vacuum chamber.

the ion beam. The propellant is injected at the rear of the channel through a high porosity mullite disk enabling a homogeneously gas diffusion. The anode is a non-magnetized stainless-steel ring placed at the back of the channel against the surface of the outer ceramic wall made of BN-SiO<sub>2</sub>. The magnetic field is generated by Sm-Co permanent-arc-segment magnets, so the magnetic field is assumed to be constant throughout the experiments (various operating conditions). The magnetic field reaches its maximum at the exit plane of the thruster channel and its minimum (close to zero) near the anode, enabling proper ionization of the propellant.

## B. Operating points

In this study we have selected three operating conditions from 150 V to 230 V to apply the keeper modulation. The operating configurations are detailed in Table 1. For all operating points, the anode and cathode flow rates remained unchanged. The equivalent mass flow rate in  $mg.s^{-1}$  for 7 SCCM and 2 SCCM of xenon is  $0.3435 mg.s^{-1}$  and  $0.0981 mg.s^{-1}$ , respectively. During the study, the thruster was not current-controlled, the gas flow rate was fixed, and different discharge voltages were studied. The cathode operated in heated mode throughout the study, i.e. with a permanent heater current.

Table 1. A review of the operating conditions with the external keeper configuration

$\phi_a$ (SCCM)	$\phi_c$ (SCCM)	Discharge current (A) - $I_d$ -	Discharge voltage (V) - $U_d$ -	Power (W)
7	2	0.476	150	73
7	2	0.498	165	82
7	2	0.516	230	118

## C. NExET chamber

All the experiments were performed in the NExET [Fig. 3] vacuum chamber (New Experiment on Electric Thrusters), the second largest facility dedicated to the study of electric propulsion, following PIVOINE-2G (national test bench for EP testing). This test bench is a  $1.8 \times 0.8$  m stainless-steel tank equipped with a primary dry pump that evacuates  $400 m^3.h^{-1}$ , a 350 l/s turbomolecular pump crucial to capture light gases like hydrogen and helium, and a cryogenic pump ( $0.5 m^2$  panel) cooled down to 45 K. Then, with the overall pumping system, we can expect a residual pressure of  $5.0 \times 10^{-5}$  mbar ( $3.75 \times 10^{-5}$  torr) while firing with xenon at  $1.2 mg.s^{-1}$ .

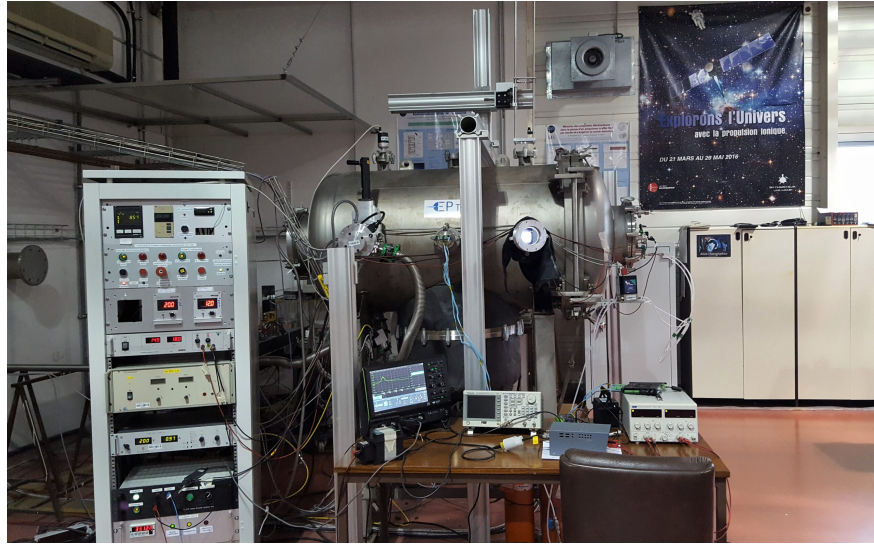


Figure 3. An image of the NExET test facility.

#### D. Langmuir probe design

A cylindrical Langmuir probe was used to capture the time varying plasma properties in the near plume of the ISCT-100-v3 Hall thruster. The probe tip was a 5 mm in length and 0.5 mm in diameter tungsten rod. The probe was installed in close proximity to the thruster exit plane at 2 cm, see Fig. 1.

The probe was polarized by a Keithley 2450 source meter to collect electron current ( $\gg V_p$ ) and ion current ( $\ll V_f$ ). Subsequently, two Teledyne Lecroy CP031A current clamps (with a bandwidth of 100 MHz) were employed to quantify the current collected by the probe over time and the discharge current. The Langmuir probe was connected to the vacuum chamber flange using shielded SMA cables for the vacuum part, and standard coaxial cables for the external part.

#### E. Modulation circuit

The objective was to design a circuit capable of amplifying a harmonic voltage signal and generating two outputs in phase opposition to obtain a non-zero potential difference. Classical electrical schematics were employed. The components utilized were procured from Apex Technology. The work of K. Dannemayer<sup>10-13</sup> on the ISCT-200, SPT-100, and PPS®1350 Hall thrusters constituted a significant source of inspiration for the circuit in question.

In addition to the aforementioned circuit, a function generator capable of generating a harmonic voltage signal at up to 20 VDC over a broad frequency range from kHz to MHz and, a battery pack to supply the electronic board (especially for the amplifiers) were utilized. This modulation system was then connected in parallel to the existing “thruster system” power supply, see Fig. 4. It is important to note that, for reasons that may be perceived as beneficial, the circuit must be floating. Consequently, an isolation transformer was incorporated between the function generator and the circuit for optimal operation. Furthermore, it is required to select amplifiers that align with the characteristics of the thruster under study.

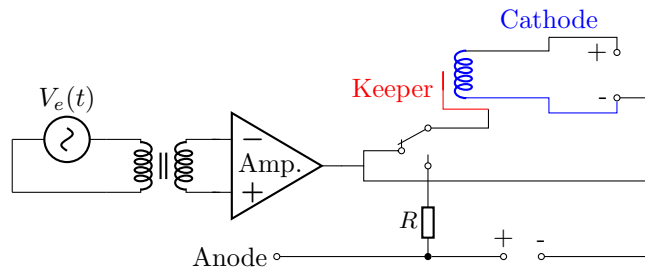


Figure 4. Schematic view of the electrical setup of the keeper electrode modulation.

Additionally, prior to the construction of the physical circuit, a simulation was conducted using LTspice<sup>®</sup> software to validate the theoretical operation of the circuit. Once developed, the circuit underwent a physical testing phase. A Teledyne Lecroy HDO 6104A oscilloscope was employed to ascertain the functionality of the circuit. The evolution of gain of the electronic board as a function of frequency is illustrated in Fig. 5 for a sinewave function ( $V_e$ ) as an input. From the aforementioned figure, it is conspicuous that the circuit response to a given input signal begins to attenuate from 400 kHz to 1 MHz, and then pursues to deteriorate up to 10 MHz. As a result, it indicates that the output signal in the MHz range no longer aligns with the theoretical signal (i.e.  $\pm 120$  V output) at MHz. It is therefore important to note that the output power at MHz is significantly lower than the output power in the kHz range.

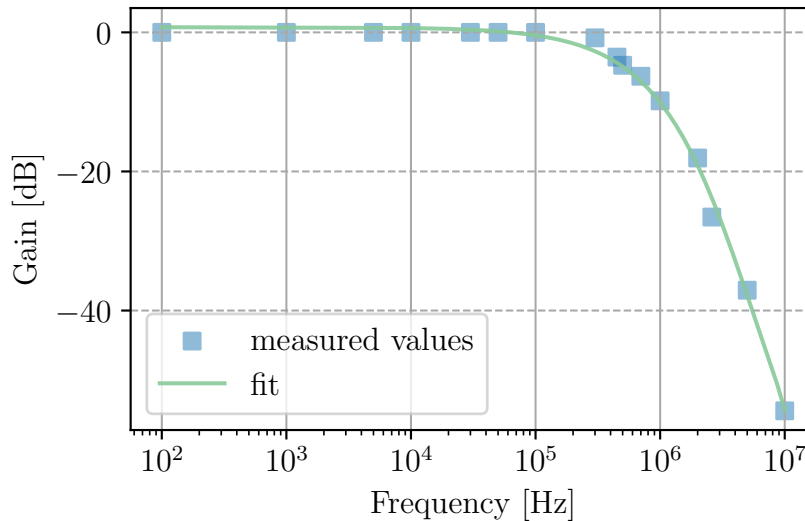


Figure 5. The evolution of the gain as a function of frequency.

### III. Results and discussion

Two mechanical configurations were tested during the experiments, namely: external keeper (electrode placed in front of the cathode orifice) and cathode-body as keeper electrode. The results presented were obtained with xenon. The protocol followed during the experiments was quite experimental (evolutionary) due to the variation of instabilities depending on the operating point studied. With the function generator providing a maximum peak-to-peak amplitude -  $V_e$  - of 12 V ( $\pm 6$  V) and a circuit with a gain of 20, the output signal is  $\pm 120$  V (240 V peak-to-peak) at maximum input amplitude. A range of amplitudes and modulation frequencies were studied. In terms of the frequency points studied, we conducted a preliminary coarse sweep (10 kHz and 100 kHz for the kHz and MHz ranges), a second moderate sweep (1 kHz and 10 kHz), and finally a third refined sweep (100 Hz and 1 kHz) as detailed in Table 2.

Table 2. A protocol for the study of modulation frequencies.

Sweep	kHz range	MHz range
coarse	10 kHz	100 kHz
moderate	1 kHz	10 kHz
refined	100 Hz	1 kHz

## A. Modulation experiments depending on keeper configuration

### 1. Experiments with the cathode-body as keeper electrode configuration

During this study, the thruster operated at 150 V and 0.5 A. Following an analysis of the discharge current (especially, the breathing mode), it was determined that a range of frequencies from 3 kHz to 18 MHz would be investigated. Once the thruster had been stabilized (thermal equilibrium), the breathing mode was established at 11.2 kHz. Regarding the modulation, the input voltage amplitudes ( $V_e$ ) ranged from 1 V to 12 V. For reasons of visibility, comprehension, and consistency, only certain magnitudes of modulation are shown.

#### a) Breathing mode modulation

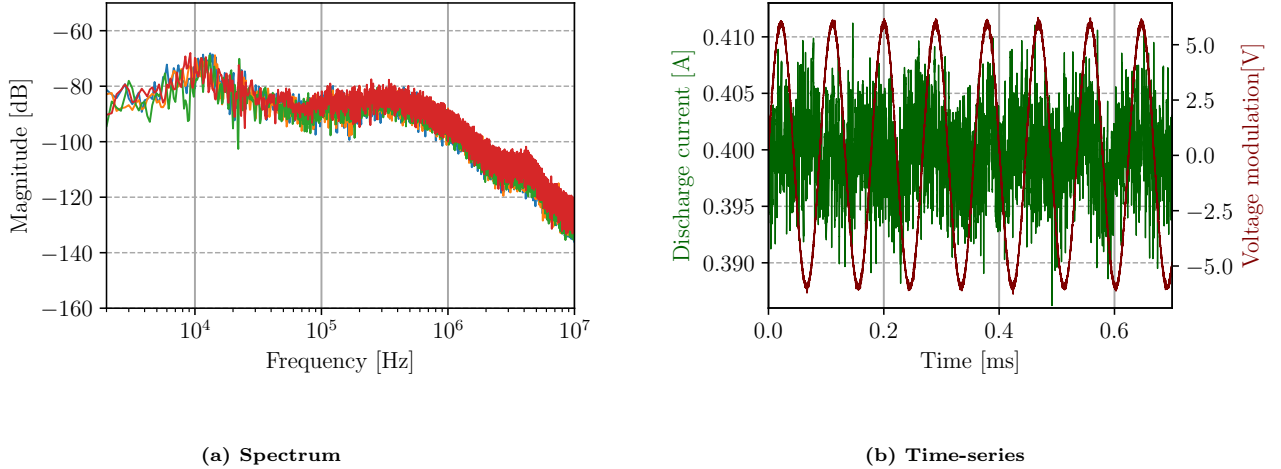


**Figure 6.** Fast Fourier transform of the reference discharge current (blue trace) and the modulated signal (other traces) for a modulation at 11.2 kHz (a), and the time evolution of the discharge current with respect to the modulation signal (b). The modulation waveform (red) is shown here before amplification. The modulation magnitude associated to the discharge current is 2 V (orange), 6 V (green), and 12 V (red).

The Fourier transform indicates in Fig. 6a that modulation is occurring, but only with an input of 12 V. Furthermore, the first harmonic is more pronounced, with a greater amplitude. Nevertheless, the effect of modulation is still barely discernible. Figure 6b displays the input signal ( $V_e$ ) sent to the circuit and compare it with the discharge current. We can then determine whether  $I_d$  (green curve) is in some way following the modulation. Thus, we will then focus on the modulations (12 V - red curve) with the most relevant frequencies. In this first case, it is not possible to conclude that the discharge current is clearly oscillating as a result of the modulation, despite the apparent correlation with the signal. In fact, we observe the natural oscillations at the same frequency as the modulation signal, rather than a smoothed amplitude or enhancement.

#### b) Modulation frequency in the breathing mode range

##### i) modulation at 3 kHz & 14 kHz:

At maximum modulation (12 V) in Fig. 7a, it is not possible to distinguish any difference between the reference signal and the “modulated” one. The Fourier transform demonstrates that the applied modulation has no impact on the discharge current.

The spectral analysis in Fig. 7b indicates that modulation at 14 kHz has a slight impact on the discharge current, with only the first harmonic visible. It can be concluded that modulation also affects discharge current outside the breathing mode, while remaining within a certain frequency range close to it. It is also worth noting that the most amplified peak is the first harmonic at 28 kHz, rather than the fundamental, which is difficult to discern. However, the amplitude is significantly lower than that of the 11.2 kHz modulation



[Fig. 6a]. It would be beneficial to ascertain whether the impact of this modulation diminishes as we move out of the range of the breathing mode.

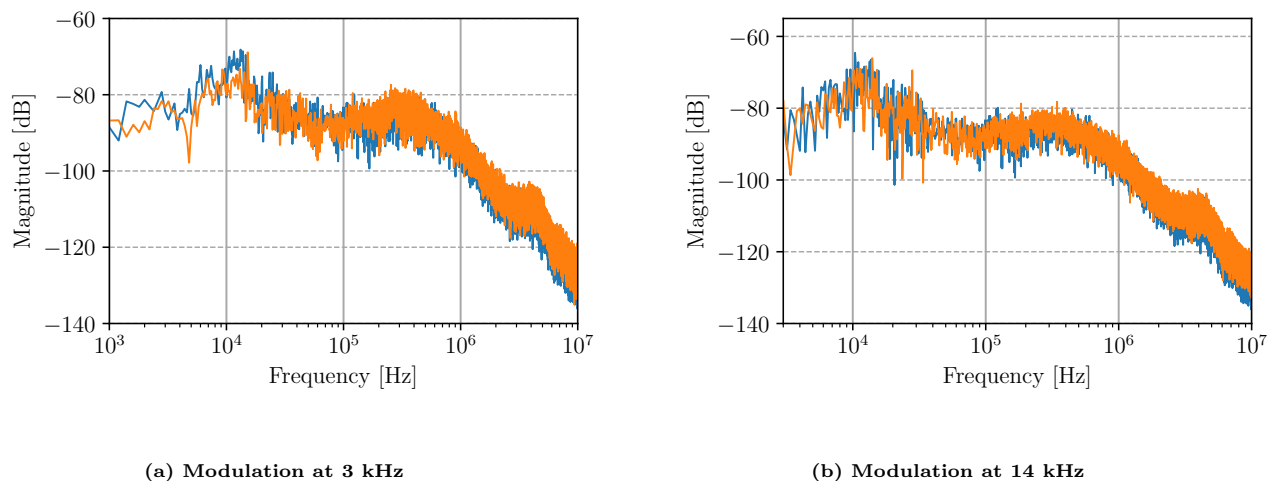


**Figure 7.** Fast Fourier Transform of the reference discharge current (blue trace) and the modulated signal (orange trace -  $V_e = 12$  V) for a modulation at 3 kHz (a) and 14 kHz (b).

*ii) modulation at 50 kHz & 573 kHz:*

We then proceeded to study the frequencies in the tens and hundreds of kilohertz. We then observed two noteworthy instances of modulation, the first at 50 kHz [Fig. 8] and the second at 573 kHz [Fig. 9]. Once again, we note the presence of modulation as indicated by the Fourier transform in Fig. 8. The signal is well modulated and the second harmonic at 150 kHz is the most amplified peak. The amplitude is greatest at the modulation maximum ( $V_e = 12$  V).

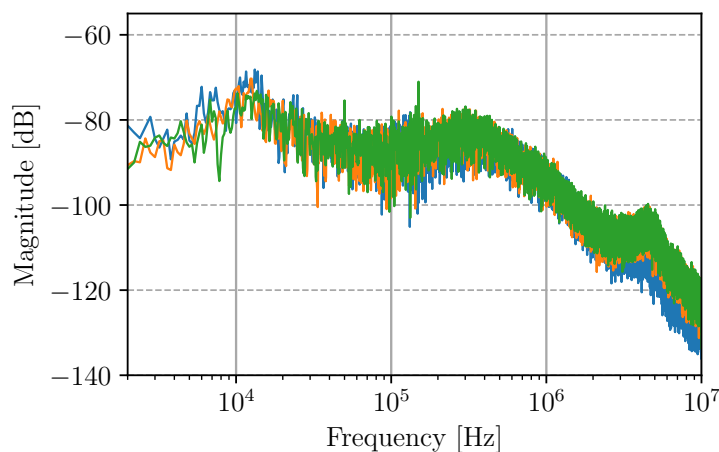
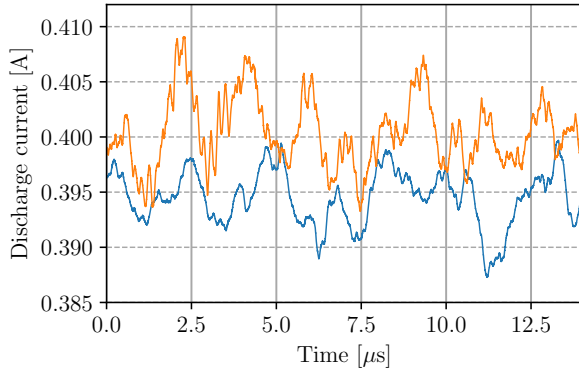
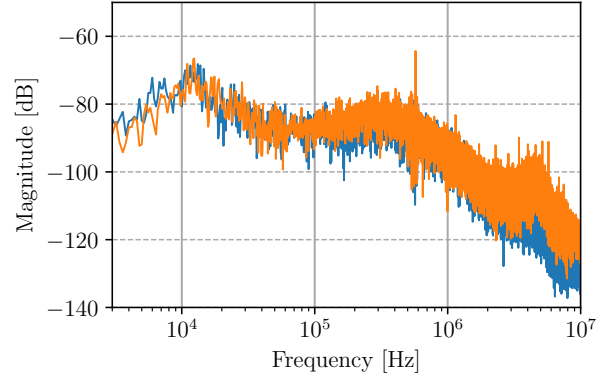


**Figure 8.** Fast Fourier Transform of the reference discharge current (blue trace) and the modulated signal (orange/green traces) for a modulation at 50 kHz. The modulation magnitude associated to the discharge current is 3 V (orange) and 12 V (green).

As illustrated in Fig. 9a, the discharge current remains relatively consistent across all curves. The presence of modulation is clearly visible in the Fourier transform in Fig. 9b and the magnitude is greater than the breathing mode. Furthermore, a multitude of harmonics are present. For this modulation frequency, we can see an amplification of an existing mode. Indeed, the amplitude amplification is significantly greater than that observed for other previously tested frequencies, such as 50 kHz.



(a) Time-series

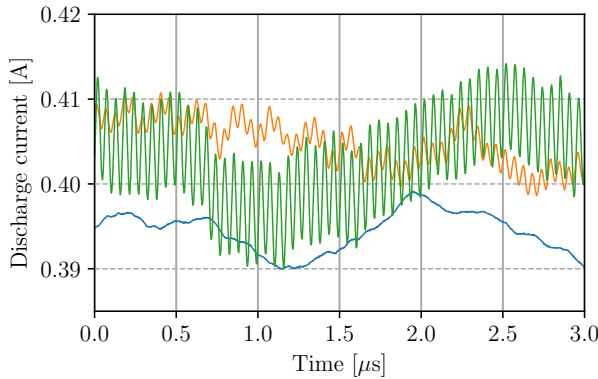


(b) Spectrum

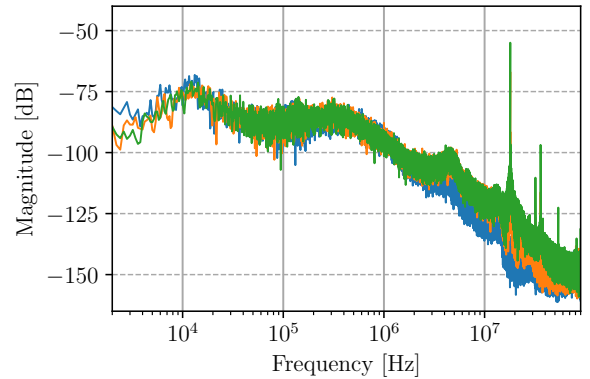
**Figure 9.** Time evolution of the modulated discharge current (orange trace -  $V_e = 12$  V) with respect to the reference (blue trace) discharge current (a), and the associated fast Fourier transform (b).

*c) High frequency modulation range*

Additionally, we sought to examine modulation at higher frequencies (MHz range). We found the modulation point at 18 MHz to be particularly interesting. The impact of modulation at high frequency is highlighted through the time series in Fig. 10a: the current oscillates more (less smoothly). As we have seen up to now, there is a broad variation in amplitude as a function of  $V_e$ . However, this became more apparent when we switched to MHz range.



(a) Spectrum



(b) Time-series

**Figure 10.** Time evolution of the modulated discharge current (orange/green traces) with respect to the reference (blue trace) discharge current (a) and the fast Fourier transform associated (b) for a modulation at 18 MHz. The modulation magnitude associated to the discharge current is 3 V (orange) and 12 V (green).

The Fourier transform in Fig. 10b indicates the presence of modulation at 18 MHz with a greater magnitude than the breathing mode. Furthermore, the harmonics are readily discernible. At this modulation frequency, we can observe the amplification of an existing mode.

## 2. Experiments with the external keeper configuration

### a) Breathing mode modulation

After reviewing the initial results obtained with the ISCT100, we determined that a second configuration would be more effective due to the low modulation of the discharge current. In previous experiments [cf. III. A. 1], the keeper was located on the cathode body. We will now be using an external electrode [Fig. 11], as K. Dannemayer exemplified this configuration in her work.<sup>10</sup> Consequently, we anticipate that implementing this modification will result in enhanced modulation outcomes. From a physics standpoint, this configuration would typically yield more impact due to enhanced field concentration (geometry and tip effect) and optimized interaction with the electron beam. Please refer to the diagram in Fig. 4 for an illustration of the actual set-up.



Figure 11. An image of the second configuration where the electrode (keeper) is placed in front of the cathode orifice without contact with the cathode-body.

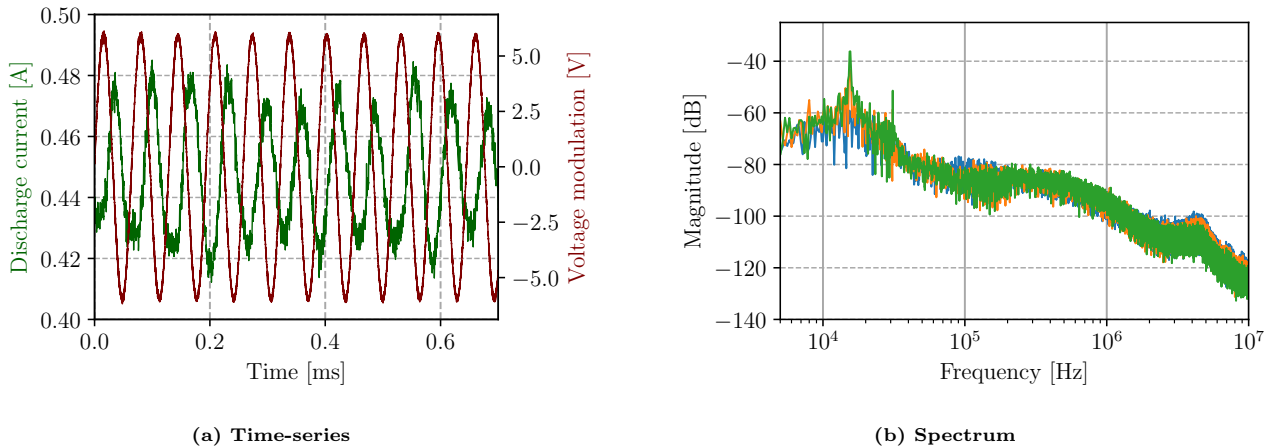


Figure 12. Time evolution of the discharge current (green) with respect to the modulation signal (a), and the fast Fourier transform of the reference discharge current (blue trace) and the modulated signal (other traces) for a modulation at 15.5 kHz. The modulation waveform (red) is shown here before amplification. The modulation magnitude associated to the discharge current is 3 V (orange) and 12 V (green).

During the experiment, the breathing mode was established at 15.5 kHz. The breathing mode is particularly evident in the graph displayed in Fig. 12b. However, modulation amplifies this effect. Furthermore, in comparison to the study conducted with the keeper on the cathode body, we observe a significant discrepancy in the impact of modulation on discharge current. The decision to use an external keeper was a positive one, as anticipated. The impact can also be seen in the time series, comparing discharge current and modulation signal. Figure 12a clearly shows the impact of modulation. In fact, the discharge current is directly influenced by the modulation signal. The oscillations are clean and stable.

### 3. Summary

In the course of this first study on the ISCT-100, we were able to examine a number of cases of modulation both via time series and spectral analysis. We particularly noted the ability to modulate the discharge current in and out of the breathing mode. In comparison with previous studies,<sup>11</sup> we can see that this time the breathing mode is only slightly impacted by modulation with the first configuration [cf. III. A. 1], and that this modulation can extend to a wide range of frequencies. The second configuration has a more pronounced impact (e.g. breathing mode), with modulation still extending over a wide range of frequencies. The modulation was visually identified by a change in the discharge oscillations and by reaching other modes (e.g. MHz). By comparing our initial modulation signal ( $V_e$ ) with the discharge current ( $I_d$ ), we observed that the latter ( $I_d$ ) closely follows the modulation, particularly in the second configuration. Furthermore, the time series confirmed that the discharge current when modulated differs from the reference current. Conversely, the mean value appears to be constant.

## B. Broad modulation study with the keeper as an external electrode

Based on the findings presented in the previous study [III. A], the current investigation will focus on the external keeper only. In this section, we sought to examine the capacity of the electronic circuit to regulate the discharge current in response to modifications in discharge voltage [Table 1]. It is therefore likely that modulation will be less effective when the discharge voltage is increased, given the modulation amplitudes we can achieve ( $\pm 120$  V). It should be noted that these operating points are not at iso power. The breathing modes obtained for the different discharge voltages are 7.5 kHz, 10.58 kHz, and 41.3 kHz, respectively.

### 1. Modulation study at different discharge voltages

#### a) Breathing mode modulation

##### i) discharge voltage at 150 V

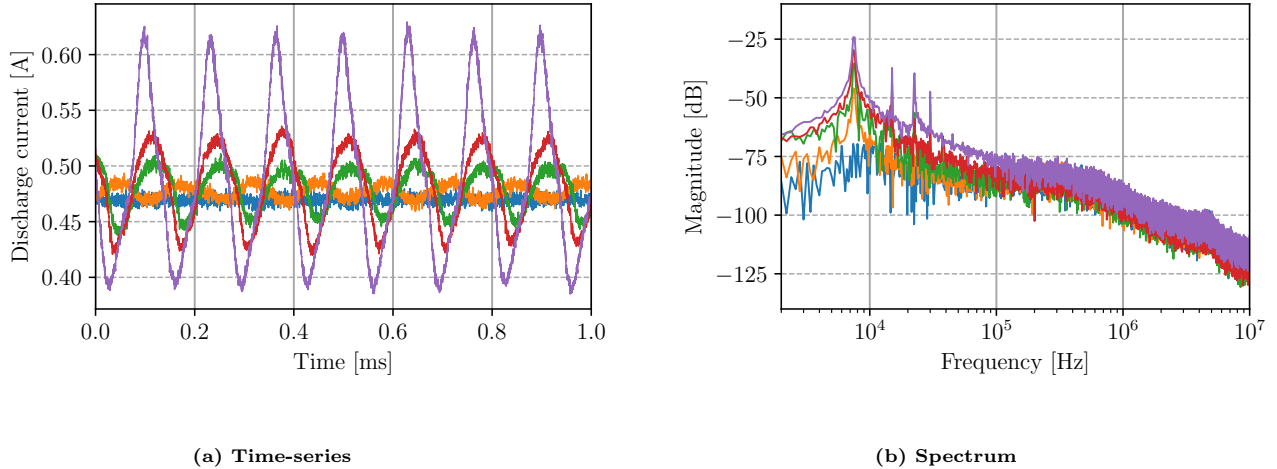


**Figure 13.** Time evolution of the modulated discharge current with respect to the reference (blue trace) discharge current (a) and the fast Fourier transform associated (b) for a modulation at 7.5 kHz. The modulation magnitude associated to the discharge current is 2 V (orange), 6 V (green), 8 V (red), and 12 V (purple).

The breathing mode is relatively low (highlighted in Fig. 13b - blue curve). However, subsequent modulation confirms its value from a visual point of view. Furthermore, in comparison with the study carried out with the keeper on the cathode body, we note an extreme difference in terms of the impact of modulation on the discharge current. This confirms the usefulness of an external keeper. We also note the clear presence of harmonics. This impact can also be seen in the time series, as shown in Fig. 13a, where the influence of the input signal amplitude is clearly visible.

*ii) discharge voltage at 165 V*

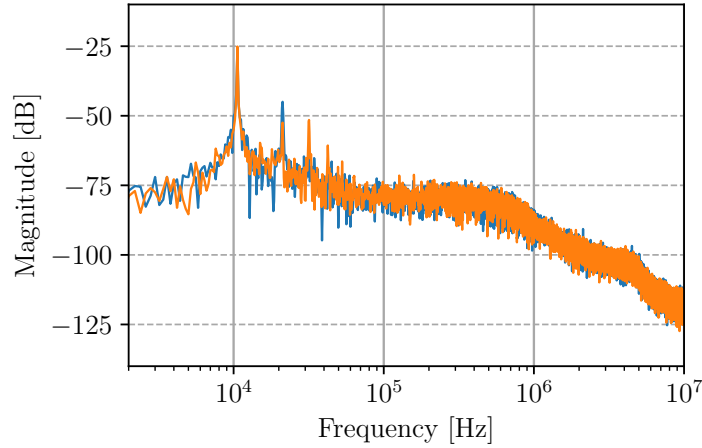


**Figure 14.** Fast Fourier transform of the discharge current for a modulation at 10.58 kHz. The modulation magnitude associated to the discharge current is 3 V (blue) and 12 V (orange).

At 160 V, we observe through a spectral analysis the impact of modulation on the breathing mode. It is displayed in Fig. 14. It is also notable that harmonics are present, although to a lesser extent than at 150 V.

*iii) discharge voltage at 230 V*

At 230 V, spectral analysis confirms a modulation in the breathing mode range [Fig. 15]. However, the difference in amplitude is minimal in comparison to the reference (blue trace). Furthermore, there are no harmonics. The results are comparable to those obtained with the keeper (1st configuration) in the previous section, but with a significantly higher discharge voltage.

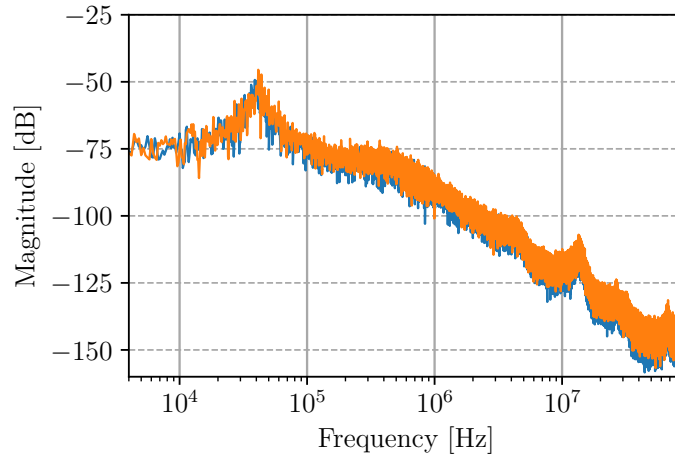


**Figure 15.** Fast Fourier transform of the reference discharge current (blue trace) and the modulated signal (orange trace -  $V_e = 12$  V) for a modulation at 41.3 kHz.

*b) Modulation before the breathing mode*

It would be beneficial to conduct further research into the modulation of the discharge current outside the breathing mode range. As a result, we conducted tests with different modulation frequencies before the breathing mode for each of the discharge voltages.

*i) discharge voltage at 150 V*

As previously demonstrated, modulation has a significant impact on the discharge current in the breathing mode. We have successfully managed to impact the discharge current before this mode [Fig. 16], which was not the case with the first keeper configuration (cathode-body). The spectral analysis in Fig. 16b has confirmed that modulation occurs at 3 kHz.

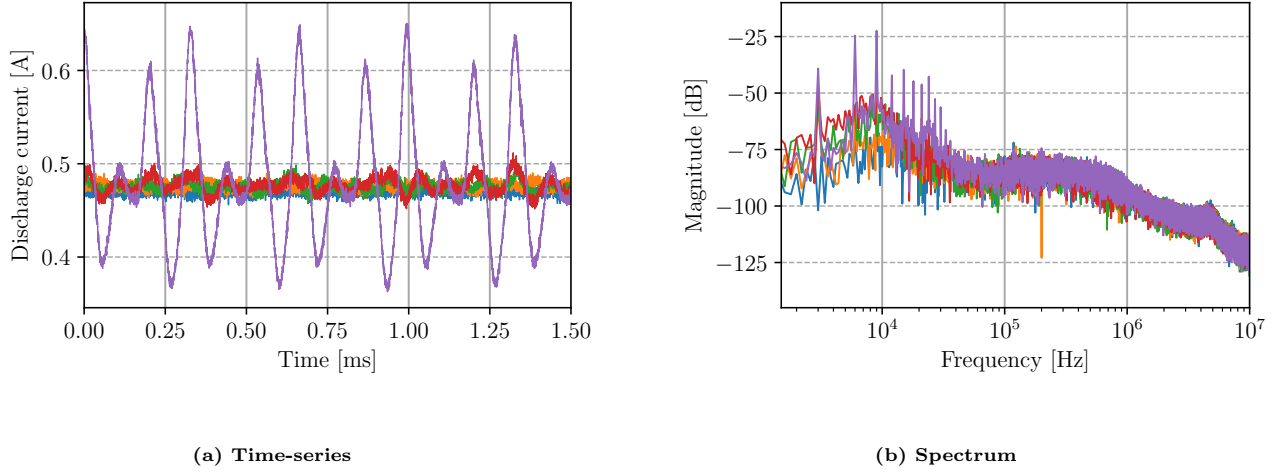


**Figure 16.** Time evolution of the modulated discharge current with respect to the reference (blue trace) discharge current (a) and the fast Fourier transform associated (b) for a modulation at 3 kHz. The modulation magnitude associated to the discharge current is 2 V (orange), 6 V (green), 8 V (red) and, 12 V (purple).

*ii) discharge voltage at 230 V*

Even though it is challenging to influence the discharge current in the breathing mode at this operating configuration, it is still possible to do so before the breathing mode, 12.5 kHz for instance in Fig. 17. This additional comparative element provides further evidence of the effectiveness of the external electrode in disrupting the discharge current.

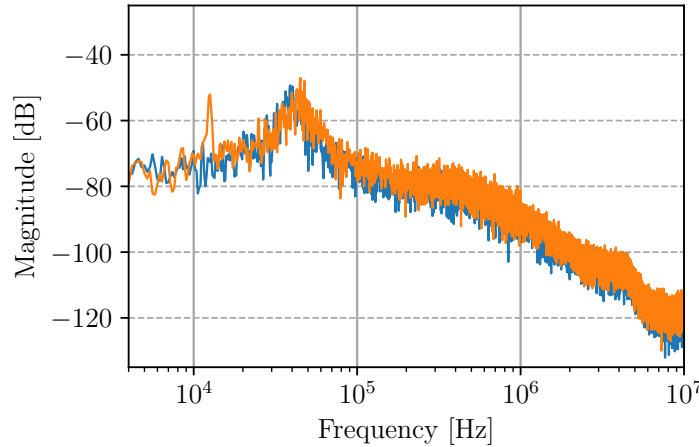


**Figure 17.** Fast Fourier transform of the reference discharge current (blue trace) and the modulated signal (orange trace -  $V_e = 12$  V) for a modulation at 12.5 kHz.

*c) Modulation beyond the breathing mode range*

Subsequently, we conducted an in-depth analysis of various frequencies beyond the breathing mode, encompassing a broad frequency spectrum from kHz to MHz. We will only provide a detailed overview of the most influential modulations.

*i) discharge voltage at 150 V*

Following a series of tests, a frequency of 18 MHz emerged as a particularly noteworthy result. This finding is corroborated by spectral analysis in Fig. 18.

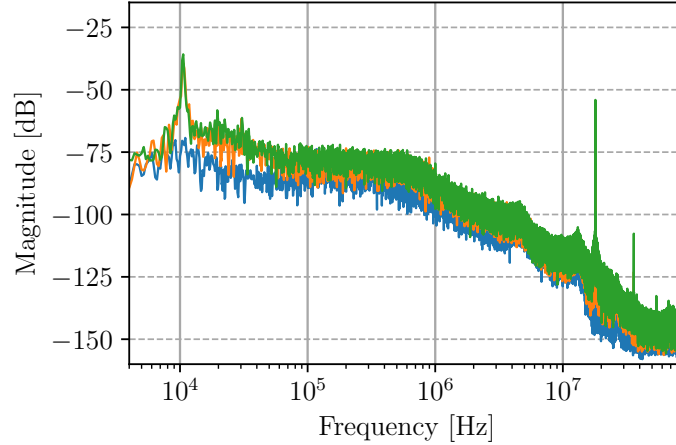


**Figure 18.** Fast Fourier transform of the reference discharge current (blue trace) and the modulated signal (orange/green traces) for a modulation at 18 MHz. The modulation magnitude associated to the discharge current is 3 V (orange) and 12 V (green).

By increasing the modulation frequency, a high-frequency mode is excited in a manner analogous to that observed when the keeper was in the first configuration [Fig. 10]. However, this time another mode is excited (the breathing mode). A comparison of the green and orange curves in Fig. 18 with the reference current data reveals that the excitation of the 18 MHz mode appears to shift the breathing mode to approximately 10 kHz (previously around 7.5 kHz). This result is of considerable interest. Indeed, it appears that there is a reciprocal relationship between two ranges of instabilities, namely the breathing mode and plasma instabilities.<sup>5</sup> Moreover, this relationship is unidirectional. It can be inferred that by controlling oscillations in the MHz range, we can influence the BM by amplifying it. It is also important to note that the power injected at these frequencies (MHz) is lower than that injected at the BM (kHz), as illustrated in the circuit characteristic diagram [cf. Fig. 5].

*ii) discharge voltage at 230 V*

Regarding the 230 V operating point, it has been determined that 22 MHz modulation is the optimal choice. The results of the spectral analysis in Fig. 19 corroborate this conclusion. Nevertheless, it is evident that the 41.3 kHz breathing mode is not amplified.

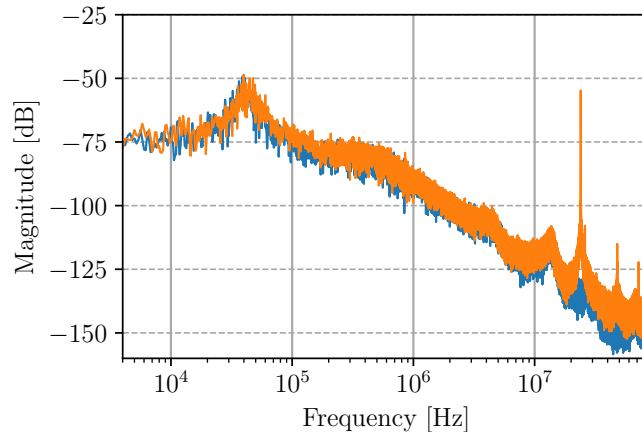


**Figure 19.** Fast Fourier transform of the reference discharge current (blue trace) and the modulated signal (orange trace -  $V_e = 12$  V) for a modulation at 22 MHz.

*d) Summary*

In conclusion, it is evident that the breathing mode (frequency) is contingent upon the discharge voltage, as demonstrated [S1-10: HET / Experiments: "Electron parameters in the plume of a 5 kW Hall thruster firing with xenon and krypton"]. Furthermore, it was observed that modulation was most effective at  $U_d = 150$  V, due to the parameters of the electronic circuit. Furthermore, the impact of the external keeper was highlighted, which extended the range of modulation action over a broader range of frequencies. The correlation between MHz and breathing mode has been repeatedly validated, including for xenon and krypton (more recently) on the same thruster with discharge voltages in the range of 150-160 V. It would be of interest to conduct a detailed study of the voltage modulation of the keeper when the discharge voltage is 150 V.

*2. Broad frequency study at 150 V*

In this subsection, we reported only the results for the 12 V input voltage modulation ( $V_e$ ) at a discharge voltage of 150 V. The measurements presented constitute a subset of the series of measurements where the breathing mode was at 15.5 kHz [Fig. 12]. These measurements were conducted subsequent to the modulation study, wherein different discharge voltages were studied (cf. III. B. 1).

*a) Electron current*

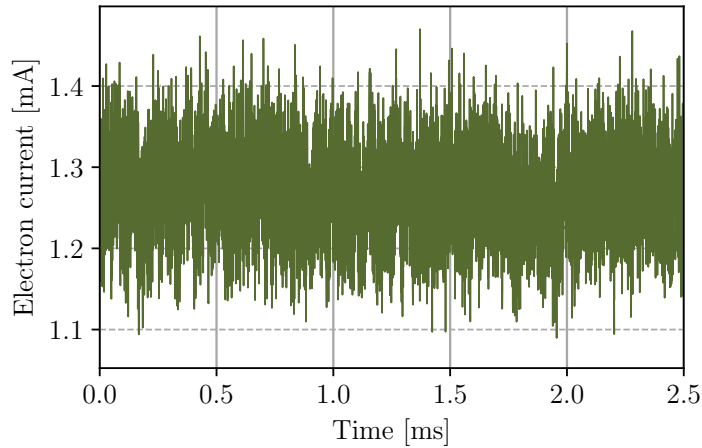


**Figure 20. Time-series of the electron current without modulation.**

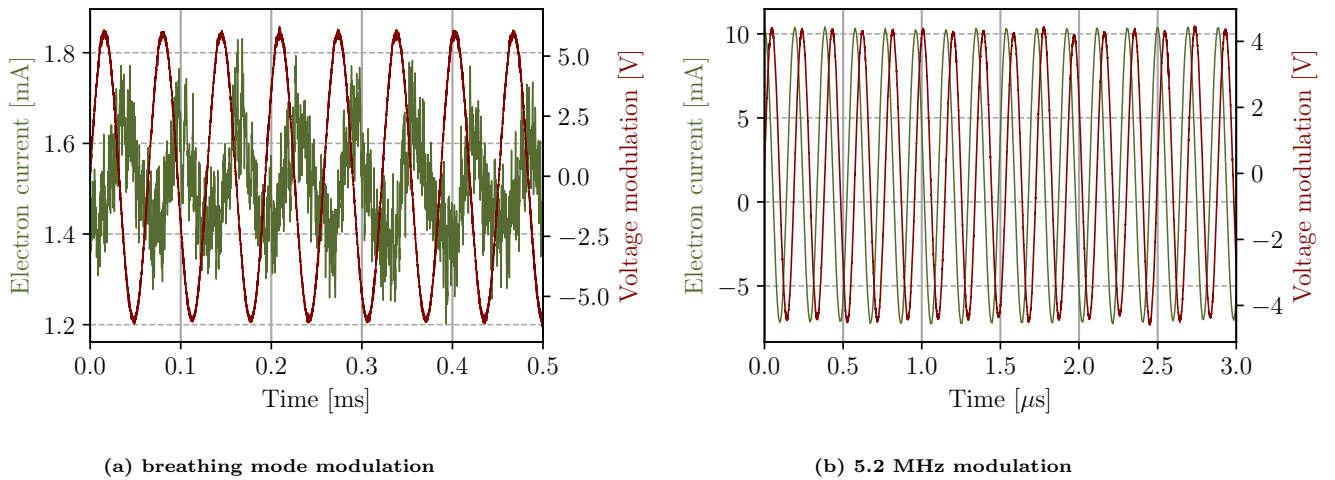


**Figure 21. Time evolution of the electron current (green) with respect to the modulation signal at the breathing mode (a), and at 5.2 MHz (b). The modulation waveform (red) is shown here before amplification.**



The objective of this study was to examine the behavior of the electron current, which, in logic, should be analogous to the discharge current. In fact, for modulation at the breathing mode, we observed a signal that accurately reflected the modulation. However, the signal exhibited greater noise than the discharge current, see Fig. 21a.

The following case, observed at 5.2 MHz in Fig. 21b, demonstrates a markedly distinct signal quality. The signal is notably clear and exhibits a precise alignment with the modulation. This has been a general observation from the outset when we compare modulation and discharge current above 5 MHz. It has been observed that the signal is noisier at low frequencies than at high frequencies. For purposes of comparison, the signal obtained for the electron current without modulation can be seen in Fig. 20.

*b) Ion current*

We can now see that the ion current is less impacted by the modulation at the breathing mode [Fig. 23a] if we compare its signal to the electron current. As the mean value is very low, so are the oscillations. This may explain the noisier signal. Nevertheless, the oscillations can be distinguished depending on the modulation signal. Furthermore, for a modulation signal above MHz [Fig. 23b], a clean, crisp signal for the ion current can be observed, as for  $I_e$  and  $I_d$ . As previously stated, the distinction between the modulated and unmodulated signals is readily apparent, as illustrated in Fig. 22.

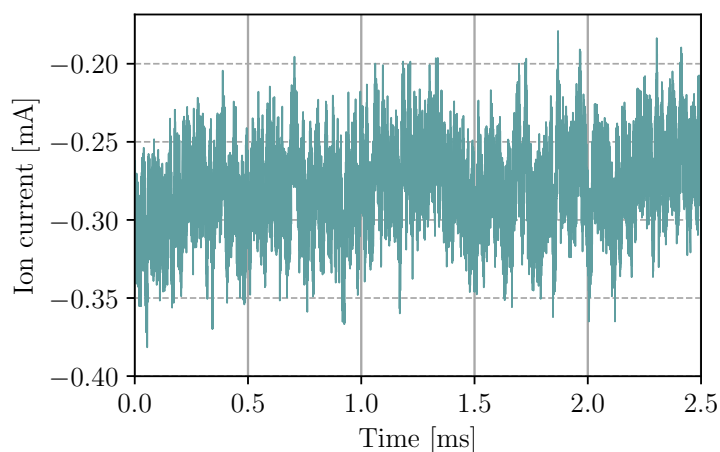


**Figure 22.** Time-series of the ion current without modulation.

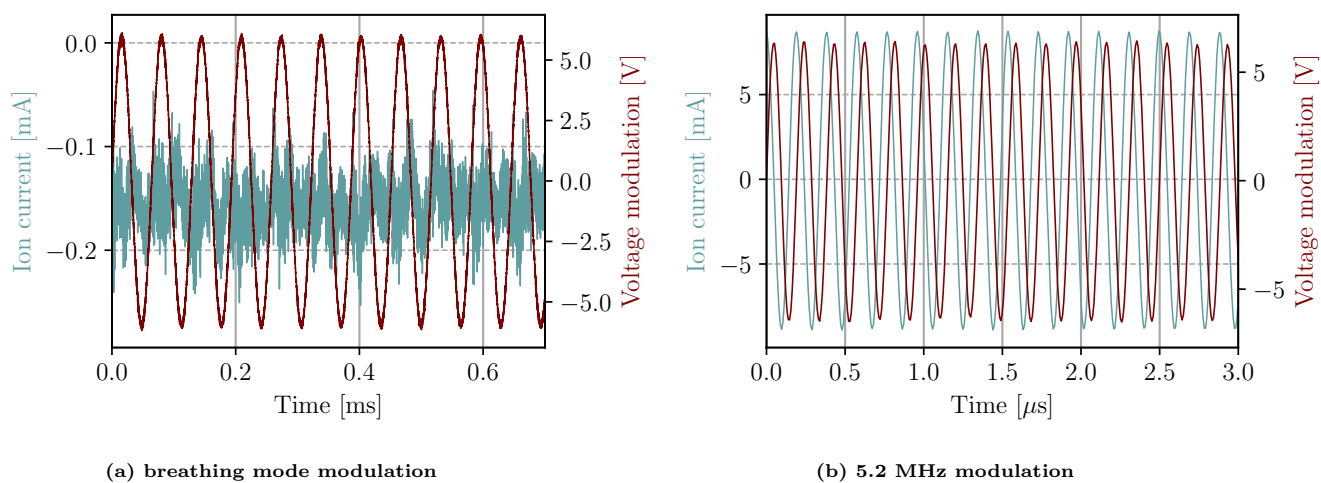


**Figure 23.** Time evolution of the ion current (cyan) with respect to the modulation signal at the breathing mode (a), and at 5.2 MHz (b). The modulation waveform (red) is shown here before amplification.

### c) Discharge and ion currents

Thus far, our research has focused on the discharge current and subsequent electron and ion currents in relation to modulation. This has enabled us to hypothesize about the effect of modulation on thruster performance. Furthermore, an additional avenue for corroborating these hypotheses would be to examine the phase relationship between the ionic and discharge currents. Indeed, as stated by J. Simmonds,<sup>7</sup> to enhance thruster performance, there should be a substantial phase difference between these two currents. For a comparison of the modulation at the breathing mode in Fig. 24a, it is unclear whether there is a phase shift. However, the signals appear to be in phase at times.

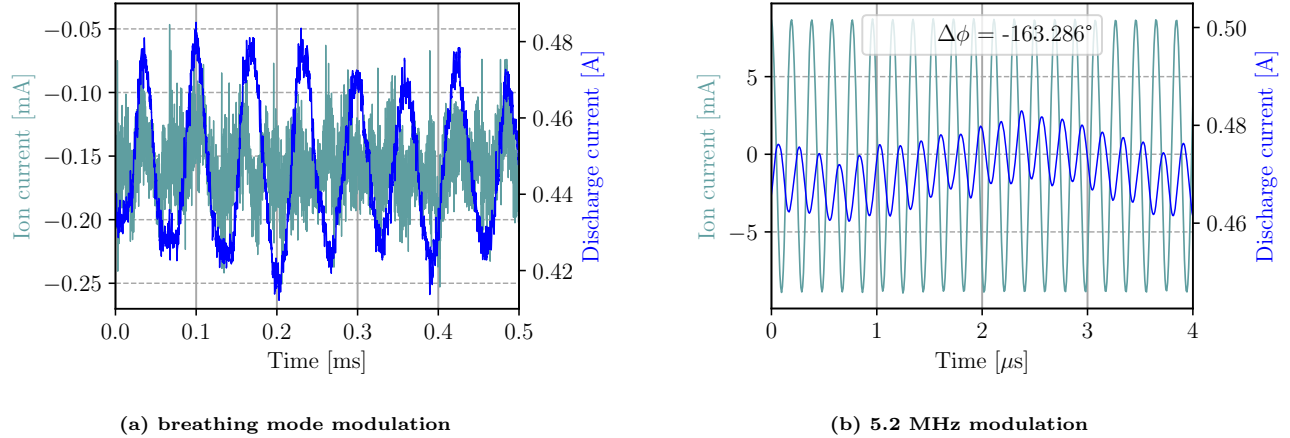


**Figure 24.** Time evolution of the ion current (cyan) with respect to the discharge current (blue) at 15.5 kHz (a) and at 5.2 MHz (b).

When comparing both currents at 5.2 MHz in Fig. 24b with the modulation at 15.5 kHz, it is evident that the ion and discharge currents are out of phase. The ion and discharge currents are approaching a  $180^\circ$  phase shift, which is positive. So, from a phase perspective, it appears that high-frequency modulation may enhance thruster performance.

## IV. Conclusion

The modulation study, conducted using multiple frequencies and voltage amplitudes, demonstrated the usefulness of the external keeper configuration over the cathode-body as keeper electrode configuration. Indeed, the results of modulation, spectral analysis, and signal comparison confirmed successful modulation at the breathing mode as well as outside, and at the MHz range. This conclusion was evident from the spectra, and further substantiated by the time-series data. The results were highly promising and demonstrated a clear correlation between modulation at MHz and breathing mode amplification. This result is particularly noteworthy, both in terms of physics and the low amount of power injected at high frequencies. Moreover, regarding all the spectra, it is noteworthy that both breathing mode and ion transit time oscillations are present at the same moment (e.g. Fig. 8).

The study of the electron current indicated that it exhibited a similar behavior to the discharge current during modulation. Regarding ion current, the impact of modulation on the breathing mode is not readily apparent. However, from the MHz onwards, the impact of modulation became evident through the analysis of the signal. Consequently, it was observed that modulation, when applied to existing or non-existing modes, provides control over discharge, electron and ion currents in some cases. Another important aspect, besides the MHz-BM correlation, is the relationship between ion current and discharge current. It would be of significant interest to ascertain whether it is possible to control the phase shift between these two currents through modulation at specific frequencies.

The impact of this modulation can be either negative or positive, depending on the circumstances. It has the potential to enhance certain performances, as evidenced by the results observed. However, to substantiate or refute these hypotheses, we must conduct a comprehensive test involving a thrust balance and a divergence study on thrusters such as the PPS®1350-ML, a higher-power Hall thruster. Once these new measurements have been established, we will be able to determine the impact of modulation on Hall thruster operation.

## Acknowledgments

This work has been supported by the French Space Agency (CNES) under grant #275049. Milan Tichý and Pavel Kudrna would like to acknowledge the partial financial support by the program Johannes Amos Comenius (co-funded by the European Union) QM4ST, project number CZ.02.01.01/00/22\_008/0004572.

## References

- <sup>1</sup>Tsikata, S., Cavalier, J., Héron, A., Honoré, C., Lemoine, N., Grésillon, D., and Coulette, D., “An axially propagating two-stream instability in the hall thruster plasma,” *Physics of Plasmas*, Vol. 21, No. 7, 7 2014, pp. 072116.
- <sup>2</sup>Katz, I., Hofer, R. R., and Goebel, D. M., “Ion current in hall thrusters,” *IEEE Transactions on Plasma Science*, Vol. 36, No. 5, 10 2008, pp. 2015–2024.
- <sup>3</sup>Kim, S. W. and Gallimore, A. D., “Plume study of a 1.35-kW SPT-100 using an EXB probe,” *Journal of Spacecraft and Rockets*, Vol. 39, No. 6, 11 2002, pp. 904–909.
- <sup>4</sup>Mazouffre, S., “Les propulseurs à plasma - une technologie spatiale d’avant-garde,” *Reflets de la physique*, , No. 14, 5 2009, pp. 15–19.
- <sup>5</sup>Boeuf, J.-P., “Tutorial: Physics and Modeling of hall thrusters,” *Journal of Applied Physics*, Vol. 121, No. 1, 1 2017, pp. 011101.
- <sup>6</sup>Boeuf, J.-P. and Garrigues, L., “Low frequency oscillations in a stationary plasma thruster,” *Journal of Applied Physics*, Vol. 84, No. 7, 10 1998, pp. 3541–3554.
- <sup>7</sup>Simmonds, J. and Raitses, Y., “Theoretical analysis of performance parameters in oscillating plasma thrusters,” *Journal of Propulsion and Power*, Vol. 37, No. 4, 7 2021, pp. 544–552.
- <sup>8</sup>Simmonds, J., Raitses, Y., Smolyakov, A., and Chapurin, O., “Studies of a modulated hall thruster,” *Plasma Sources Science and Technology*, Vol. 30, No. 5, 5 2021, pp. 055011.
- <sup>9</sup>Romadanov, I., Raitses, Y., and Smolyakov, A., “Hall thruster operation with externally driven breathing mode oscillations,” *Plasma sources science and technology*, Vol. 27, No. 9, 9 2018, pp. 094006.
- <sup>10</sup>Dannenmayer, K., “Scaling laws and electron properties in hall effect thrusters,” <https://tel.archives-ouvertes.fr/tel-00797732/>, 10 2012.
- <sup>11</sup>Dannenmayer, K., Kudrna, P., Tichý, M., and Mazouffre, S., “Time-resolved measurement of plasma parameters in the far-field plume of a low-power Hall effect thruster,” *Plasma Sources Science and Technology*, Vol. 21, No. 5, 9 2012, pp. 055020.
- <sup>12</sup>Dannenmayer, K., Kudrna, P., Tichý, M., and Mazouffre, S., “Time-Resolved measurements of plasma properties using electrostatic probes in the Cross-Field discharge of a hall effect thruster,” *Contributions To Plasma Physics*, Vol. 53, No. 1, 1 2013, pp. 63–68.
- <sup>13</sup>Dannenmayer, K., Mazouffre, S., Kudrna, P., and Tichý, M., “The time-varying electron energy distribution function in the plume of a hall thruster,” *Plasma Sources Science and Technology*, Vol. 23, No. 6, 8 2014, pp. 065001.
- <sup>14</sup>Vaudolon, J., Mazouffre, S., Hénaux, C., Harribey, D., and Rossi, A., “Optimization of a wall-less hall thruster,” *Applied Physics Letters*, Vol. 107, No. 17, 10 2015, pp. 174103.
- <sup>15</sup>Szabo, J. J., Tedrake, R., Metivier, E., Paintal, S., and Taillefer, Z., “Characterization of a One Hundred Watt, Long Lifetime Hall Effect Thruster for Small Spacecraft,” *53rd AIAA/SAE/ASEE Joint Propulsion Conference*, 7 2017.
- <sup>16</sup>Mazouffre, S., “Propulseur ISCT100 v3 – Aleph Zero,” 10 2018.
- <sup>17</sup>Vincent, B., Tsikata, S., Potrivitu, G.-C., Garrigues, L., Sary, G., and Mazouffre, S., “Electron properties of an emissive cathode: analysis with incoherent thomson scattering, fluid simulations and Langmuir probe measurements,” *Journal of physics. D, Applied physics*, Vol. 53, No. 41, 7 2020, pp. 415202.